

# Domain supersolids in binary dipolar condensates

T. Bland,<sup>1,2</sup> E. Poli,<sup>2</sup> L. A. Peña Ardila,<sup>3</sup> L. Santos,<sup>3</sup> F. Ferlaino,<sup>1,2</sup> and R. N. Bisset<sup>2</sup>

<sup>1</sup>*Institut für Quantenoptik und Quanteninformation,*

*Österreichische Akademie der Wissenschaften, Innsbruck, Austria*

<sup>2</sup>*Institut für Experimentalphysik, Universität Innsbruck, Austria*

<sup>3</sup>*Institut für Theoretische Physik, Leibniz Universität Hannover, Germany*

(Dated: March 22, 2022)

Two-component dipolar condensates are now experimentally producible, and we theoretically investigate the nature of supersolidity in this system. We predict the existence of a binary supersolid state in which the two components form a series of alternating domains, producing an immiscible double supersolid. Remarkably, we find that a dipolar component can even induce supersolidity in a nondipolar component. In stark contrast to single-component supersolids, the number of crystal sites is not strictly limited by the condensate populations, and the density is hence substantially lower. Our results are applicable to a wide range of dipole moment combinations, marking an important step towards long-lived bulk-supersolidity.

The once elusive supersolid state of matter simultaneously exhibits superfluidity and crystalline order [1]. Ultimately, it was the high-degree of flexibility and control offered by ultracold gases that finally led to its observation in recent groundbreaking experiments. Supersolid properties were observed in systems with spin-orbit coupling [2, 3] and cavity-mediated interactions [4], although there the crystals were rigid and unexcitable in the usual sense. Supersolids with genuinely deformable crystals were finally observed with dipolar Bose-Einstein condensates (BECs) [5–7], and their excitations were confirmed soon after [8–10].

Dipolar supersolids may be created from unmodulated BECs by inducing a roton instability [5–7]. Roton excitations—with a finite wavelength governed by the anisotropic and long-ranged dipole-dipole interactions [11, 12]—were first observed in cigar-shaped [8, 13] and then in pancake-shaped BECs [14]. An unstable roton mode seeds a periodic density modulation that can subsequently be stabilized by quantum fluctuations, which become increasingly important as the density grows, resulting in an array of quantum droplets [15, 16]. Indeed, the present generation of supersolids can be thought of as droplet arrays with a continuous superfluid connection and global phase coherence. For this reason, we will hereon refer to these as *droplet supersolids* to distinguish them from the *domain supersolids* that we will introduce shortly. Droplet supersolids were first realized in cigar-shaped traps, producing linear arrays of droplets [5–7], whereas experiments have now also created 2D droplet supersolids [17, 18]. From a theoretical perspective, there have been intriguing predictions for exotic supersolid states [19–23], as well as alluring manifestations of quantum vortices [24–26].

It is now possible to experimentally produce BEC mixtures of highly-magnetic erbium and dysprosium atoms [27–29], and the extra degrees of freedom open numerous possibilities for supersolidity. In Ref. [30] it was proposed that two immiscible BECs—displaced relative to one an-

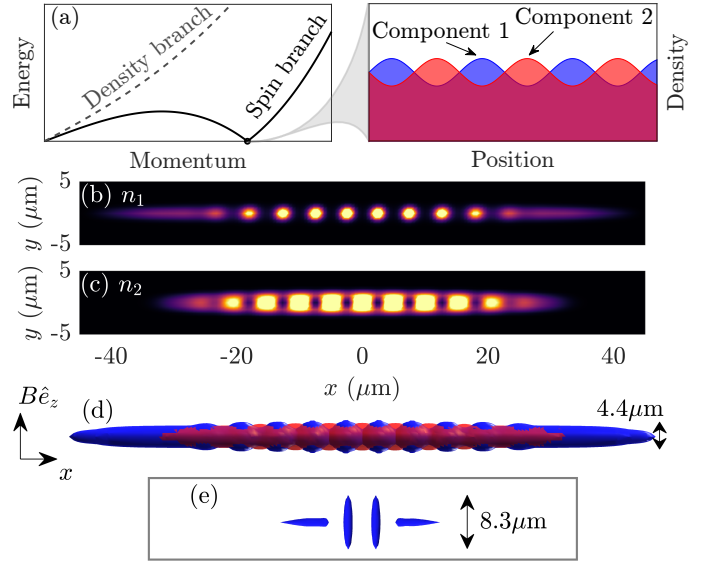


FIG. 1. (a) Dispersion relation schematic showing a roton instability in the spin branch with corresponding density modulations on the right. (b-d) Domain supersolid for a dysprosium dipolar-nondipolar mixture. Column densities for (b) dipolar and (c) nondipolar components, with (d) double-isosurface plotted at 2% of the peak density for each component. Interaction scattering lengths  $(a_{11}, a_{12}, a_{22}) = (100, 98, 100)a_0$ , trapping frequencies  $\vec{f} = (5, 110, 150)\text{Hz}$ , and populations  $N_1 = N_2 = 1.5 \times 10^4$ . (e) Corresponding single component dipolar droplet crystal for the same trapping potential,  $N = 3 \times 10^4$  and  $a = 78a_0$ . Subplots (b-e) are drawn to the same length scale.

other by non-concentric confinement—might be used to realize a kind of binary supersolid formed by the instability of interface bending modes. More recently, it has been predicted that exotic droplet supersolid states can be seeded by the addition of a second dipolar component [29, 31]. Binary dipolar condensates also present another intriguing possibility. It has already been predicted that unmodulated binary BECs may be destabilized by spin

roton excitations [32] (also see [33]), for which a periodic density modulation of one component develops out of phase with the other, as depicted in Fig. 1(a). Then, in analogy to a roton instability producing a droplet supersolid, could the unstable spin rotons point to the existence of a binary supersolid phase consisting of alternating domains?

In this letter, we theoretically investigate the possibility for supersolidity in two-component (pseudo-spin 1/2) dipolar BECs in regimes where quantum droplets are absent. We predict the existence of *domain supersolids* in which the components form alternating domains, with a continuous superfluid connection within each component that periodically weaves through the other [see Fig. 1 (b-d)]. We uncover rich phase diagrams with a domain supersolid state occurring over broad regions of parameter space. On one side of the double supersolid region there lies a phase transition to the unmodulated miscible state, while on the other side the system transitions to a single supersolid state that is periodically punctuated by the isolated domains of the second component. We generalize our results to various dipole strength combinations, broadly applicable to spin mixtures or combinations of different atomic species, and demonstrate that the domain supersolid intrinsically relies on the imbalance between the two dipole moments. Interestingly, we find that a dipolar component can even induce supersolidity in a nondipolar component. We find that the domains may have atom numbers and peak densities far below the threshold required for droplet formation, which has important implications for the potential size of supersolid crystals in realistic settings, as well as for their longevity, which is largely determined by the inelastic 3-body collisions that depend strongly on the density [16].

*Formalism.*—We consider a three-dimensional system at zero temperature made of two bosonic components,  $\sigma = \{1, 2\}$ , consisting of atoms with permanent magnetic moments, although our work is also applicable to electric dipoles. Following Refs. [34, 35], we compute the Lee-Huang-Yang (LHY) energy density correction due to quantum fluctuations for a homogeneous binary mixture with densities  $\mathbf{n} = (n_1, n_2)$ :

$$\epsilon_{\text{LHY}}(\mathbf{n}) = \frac{16}{15\sqrt{2\pi}} \left( \frac{m}{4\pi\hbar^2} \right)^{3/2} \int_0^1 du \sum_{\lambda=\pm} V_{\lambda}(u, \mathbf{n})^{5/2}, \quad (1)$$

where we assume equal masses  $m = m_1 = m_2$ , and

$$V_{\pm}(u, \mathbf{n}) = \sum_{\sigma=1,2} \alpha_{\sigma\sigma} n_{\sigma} \pm \sqrt{(\alpha_{11}n_1 - \alpha_{22}n_2)^2 + 4\alpha_{12}^2 n_1 n_2}. \quad (2)$$

Here,  $\alpha_{\sigma\sigma'}(u) = g_{\sigma\sigma'} + g_{\sigma\sigma'}^d(3u^2 - 1)$ , where the short-ranged and dipolar interaction parameters are, respectively,  $g_{\sigma\sigma'} = 4\pi\hbar^2 a_{\sigma\sigma'}/m$  and  $g_{\sigma\sigma'}^d = \mu_0\mu_{\sigma}\mu_{\sigma'}/3 =$

$4\pi\hbar^2 a_{\sigma\sigma'}^d/m$ , with  $s$ -wave scattering lengths,  $a_{\sigma\sigma'}$  and dipole moments  $\mu_{\sigma}$ , where  $\mu_0$  is the vacuum permeability. The wave function for each component  $\Psi_{\sigma}$  is obtained by solving the coupled extended Gross-Pitaevskii equations:

$$i\hbar \frac{\partial}{\partial t} \Psi_{\sigma}(\mathbf{x}) = \left[ -\frac{\hbar^2 \nabla^2}{2m} + \frac{1}{2}m(\omega_x^2 x^2 + \omega_y^2 y^2 + \omega_z^2 z^2) + \sum_{\sigma'} \int d^3r' U_{\sigma\sigma'}(\mathbf{x}' - \mathbf{x}) n_{\sigma'}(\mathbf{x}') + \sum_{\sigma'} g_{\sigma\sigma'} n_{\sigma'}(\mathbf{x}) + \mu_{\text{LHY}}^{(\sigma)}[\mathbf{n}(\mathbf{x})] \right] \Psi_{\sigma}(\mathbf{x}), \quad (3)$$

where  $\omega_{x,y,z} = 2\pi f_{x,y,z}$  are the harmonic trapping frequencies,  $U_{\sigma\sigma'}(\mathbf{r}) = [\mu_0\mu_{\sigma}\mu_{\sigma'}/4\pi r^3] (1 - 3\cos^2\theta)$  is the long-ranged anisotropic dipole-dipole interaction potential, with  $\theta$  the angle between the polarization axis (always  $z$ ) and the vector  $\mathbf{r}$  that connects the two interacting particles, and  $n_{\sigma}(\mathbf{x}) \equiv |\Psi_{\sigma}(\mathbf{x})|^2$  is the density of component  $\sigma$ , normalized to  $N_{\sigma}$  atoms. The last term in (3) is the quantum fluctuation correction to the chemical potential  $\mu_{\text{LHY}}^{(\sigma)}[\mathbf{n}(\mathbf{x})] = \partial\epsilon_{\text{LHY}}(\mathbf{n}(\mathbf{x}))/\partial n_{\sigma}$ , described within the local-density approximation framework.

*Domain supersolids.*—We demonstrate the unique features of domain supersolids by considering a dipolar-nondipolar mixture in Fig. 1, for which a combined total of 19 domains can be seen. While the dipolar component [Fig. 1(b)] can remain globally phase coherent through a continuous superfluid connection linking the domains—since we are close to the miscible-immiscible phase transition the separation is only partial—the nondipolar component [Fig. 1(c)] can also maintain a superfluid connection along high density rails encompassing the dipolar domains. The density isosurfaces in Fig. 1(d) highlight the shape of the dipolar domains, which are not strongly elongated, as opposed to dipolar droplets [cf. Fig. 1(e)]. While this concrete illustration considers two  $^{164}\text{Dy}$  spin projections, with  $(\mu_1, \mu_2) = (-10, 0)\mu_B$  for Bohr magneton  $\mu_B$ , domain supersolids are not just a special feature of dipolar-nondipolar mixtures, but are rather general, as we discuss later.

These results must be contrasted to the single-component case. In Fig. 1(e) we show a droplet crystal for a single-component dipolar BEC for the same trap and total atom number as in Fig. 1(b-d), i.e.,  $N = 3 \times 10^4$ . Note that we had to modify the scattering length, since  $a = 100a_0$  corresponds to an unmodulated BEC. However, lowering to  $a = 78a_0$  passes a phase transition directly to a pair of isolated droplets and a low density halo, with a peak density ( $4.0 \times 10^{21} \text{ m}^{-3}$ ) more than an order of magnitude larger than the domain supersolid case ( $1.8 \times 10^{20} \text{ m}^{-3}$ ). Correspondingly, the number of atoms per lattice site is about an order of magnitude larger than for the domain supersolid. For this atom number and trap volume, the droplet supersolid phase does not exist for the single-component case [23], which was also the situation for the regimes considered by Refs. [36–38].

To understand the physical mechanisms involved, it is instructive to consider the transition from unmodulated to modulated states. For the formation of a domain supersolid, the density modulation is triggered by unstable spin roton excitations [Fig. 1(a)], with wavelengths governed by the BEC's width along the direction of dipole polarization [39]. Spin modes tend to maximize the density difference,  $|n_1 - n_2|$ , and the instability is hence partially resolved once the components become spatially separated as alternating immiscible domains [Figs. 1(b-d)]. Crucially, there is no implosion of total density,  $n_1 + n_2$ , and the peak density can remain low. This situation should be contrasted to that for droplet supersolids, in which roton excitations trigger local implosions of the total density, and these are only stabilized once a significantly higher density is reached in a process called quantum stabilization [37, 38, 40], underpinned by the single-component limit of Eq. (1). It is important to note that while quantum fluctuations (1) are not strictly required to stabilize domain supersolids at much higher intraspecies scattering lengths, they remain qualitatively important for the regimes considered in this work. For example, if quantum fluctuations were neglected for the regime of Figs. 1(b-d) we find a runaway implosion of the dipolar domains (not shown).

Each component within the binary system exists in one of three phases: an unmodulated BEC, a supersolid state with a linear chain of domains (SS), or an array of isolated domains (ID). The distinction between these phases is set by the density contrast  $C_\sigma = (n_\sigma^{\max} - n_\sigma^{\min}) / (n_\sigma^{\max} + n_\sigma^{\min})$ , where  $n_\sigma^{\max}$  and  $n_\sigma^{\min}$  are neighboring maxima and minima as one moves along the long direction of the trap [41]. In this work we take  $0 < C_\sigma < 0.98$  to be a supersolid, and  $C_\sigma > 0.98$  to be isolated domains. We focus on regimes where the stationary state solution of one component without the presence of the other will always be unmodulated ( $C_\sigma = 0$ ). For reference, the contrasts in Fig. 1 are (b)  $C_1 = 0.9527$ , (c)  $C_2 = 0.6097$ , and (e)  $C_1 = 0.9998$ .

*Phase diagram for dipolar-nondipolar mixture.*—In Fig. 2 we explore the stationary state phase diagram of a dipolar-nondipolar mixture in a cigar-shaped trap with  $(f_x, 150, 150)$ Hz,  $N_1 = N_2 = N/2$  and fixed  $Nf_x = 3 \times 10^5$ Hz to maintain an approximately constant average density [23]. At low  $a_{12} \lesssim 60a_0$  the stationary state solution is a miscible unmodulated BEC, with only small deviation from perfect density overlap between components due to magnetostriction in the dipolar component [Fig. 2■]. Increasing  $a_{12}$  induces a transition to a domain supersolid state (SS-SS) [Fig. 2▲], where the domains of a given component exhibit a continuous superfluid connection [ $C_\sigma < 0.98$  in Figs. 2(b)(c)]. We find that a quench of the intercomponent scattering length from the unmodulated miscible state to the domain supersolid regime generates a globally phase-coherent state—within each component—that is robust against the excitations

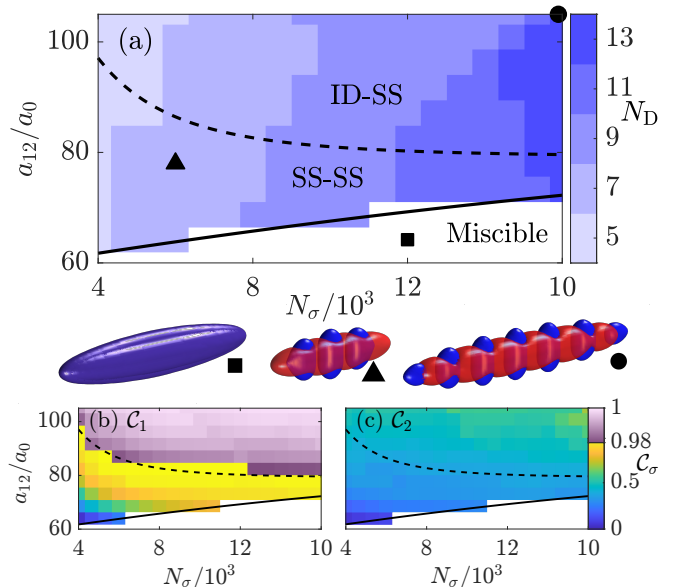


FIG. 2. Phase diagram for a dipolar-nondipolar mixture of  $^{164}\text{Dy}$  atoms, varying intercomponent scattering length  $a_{12}$  and  $N_1 = N_2 = N/2$  with fixed  $Nf_x$ , from  $f_x = 37.5$ Hz on the left to  $f_x = 15$ Hz on the right. (a) Total number of domains in the stationary state solution. Solid lines separate miscible to domain supersolid (SS-SS) state, and dashed line to isolated domains-supersolid (ID-SS) state. Example isosurfaces below are highlighted by the symbols in (a). (b,c) Density modulation contrast  $C_\sigma$  of components 1 and 2. Threshold between SS and ID regime is indicated by a change of color scale. Other parameters:  $a_{11} = a_{22} = 100a_0$ ,  $(\mu_1, \mu_2) = (-10, 0)\mu_B$ ,  $f_y = f_z = 150$ Hz.

induced by the quench, in-keeping with studies of droplet supersolids in a cigar-shaped geometry [5–7], which we detail in the Supplemental Materials [42, 43]. Note how broad the SS-SS regime is, at least  $10a_0$  wide, compared to droplet supersolids where it is typically only a few  $a_0$  wide. Further increasing  $a_{12}$  causes the overlap between components to reduce, expanding the distance between domains whilst increasing the contrast [Fig. 2(b)], crossing into the isolated domain-supersolid (ID-SS) regime [Fig. 2●]. However, the nondipolar component maintains a strong superfluid connection [Fig. 2(c)]. Note that the superfluid connection of component 2 can be controlled by adjusting  $f_y$ , with even a small reduction in  $f_y$  significantly reinforcing the nondipolar rails around the dipolar domains.

Figure 2(a) also shows how the total number of domains  $N_D$  changes in this phase diagram. Throughout, the average atom number per domain is  $\sim 10^3$ . Hence, as the atom number increases the number of domains climbs steadily, reaching a total of 13 once the system has  $2 \times 10^4$  atoms ( $10^4$  per component) on the far right-hand side. In contrast, droplet supersolids typically require  $\sim 10^4$  atoms per droplet [5–7].

*Generalization to various dipole combinations.*— Here,

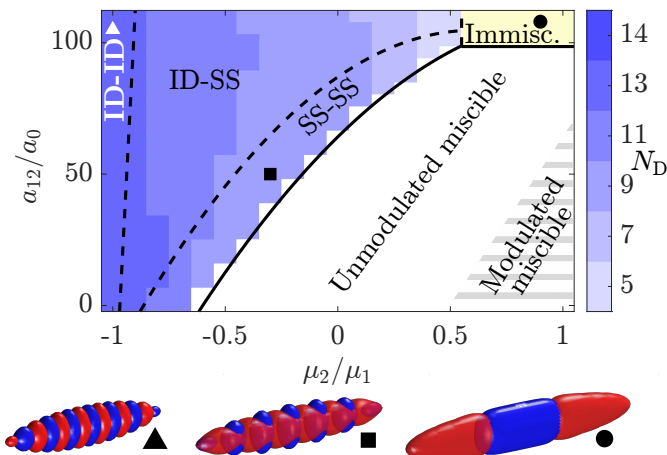


FIG. 3. Phase diagram for dipolar mixtures with varying inter-component scattering length and relative magnetic moment (note that  $\mu_2/\mu_1 < 0$  implies antiparallel dipoles). Compared to Fig. 2, note the new phases: binary isolated domains (ID-ID), macroscopic-domain immiscibility (beige region), and the modulated miscible regime [31]. Parameters:  $N_1 = N_2 = 5 \times 10^3$ ,  $a_{11} = a_{22} = 100a_0$ , and  $(f_x, f_y, f_z) = (15, 150, 150)\text{Hz}$ .

we generalize our findings to mixtures in which both components can be dipolar, applicable to a wide range of experiments, e.g., erbium-dysprosium mixtures or spin mixtures of the same species. In Fig. 3, we construct a phase diagram by fixing  $\mu_1$  and exploring the effect of varying  $\mu_2$  and  $a_{12}$ . A solid line indicates a transition from a miscible to immiscible state, consistent with Fig. 2. For  $\mu_2/\mu_1 < 0$  the dipoles are anti-aligned, decreasing the energy for dipoles of separate components to orient in the side-by-side configuration, thus causing both immiscibility and domain supersolidity to occur at low  $a_{12}$  [Fig. 3 ■]. At  $\mu_2/\mu_1 = -1$  the modulation is a perfect reflection about the  $x = 0$  plane between the components, and for the range of  $a_{12}$  considered the system forms a binary isolated domain (ID-ID) state with 14 domains for only  $10^4$  atoms in total [Fig. 3 ▲].

For similar dipoles  $\mu_2 \sim \mu_1$  there is little energy incentive from the dipolar interactions for the components to phase separate [33], hence the immiscibility boundary in Fig. 3 is close to the nondipolar result  $a_{12} = \sqrt{a_{11}a_{22}} = 100a_0$ , and the components separate to a macroscopic-domain immiscible state [39] [Fig. 3 ●]. While we focus on the immiscible domain regime, smaller  $a_{\sigma\sigma}$  would trigger the formation of immiscible droplet supersolids [29, 31]. Miscible droplet supersolids are also possible for smaller  $a_{12}$ , as shown in the bottom right-hand corner of Fig. 3, which is explored further in Ref. [31].

*Ultra-low density supersolids.*— We investigate weakening the axial confinement of a dipolar-nondipolar spin mixture of erbium, further demonstrating the generality of our results to a broad range of dipole combinations. On the far right of Fig. 4 is a state in the ID-SS regime

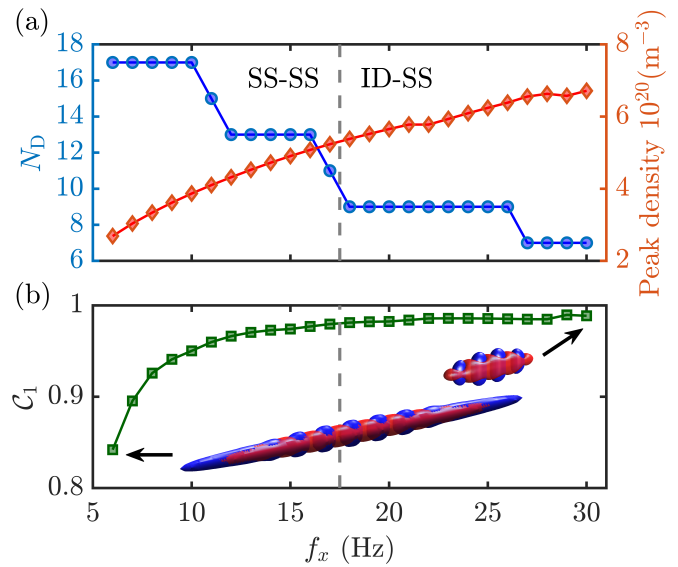


FIG. 4. Opening the trap for an erbium dipolar-nondipolar supersolid. (a) Reducing the long axis trap frequency,  $f_x$ , of a cigar-shaped trap increases the number of domains  $N_D$  whilst simultaneously reducing the peak density. (b) Contrast of the dipolar component also reduces, indicating an improving superfluid connection, whilst the second component is always a robust supersolid with its contrast never exceeding 0.6 (not shown). The dashed line indicates a transition from the SS-ID regime to the SS-SS regime. Parameters:  $\mu_1 = -7\mu_B$  and  $\mu_2 = 0$ ,  $(a_{11}, a_{12}, a_{22}) = (65, 60, 65)a_0$ ,  $N_1 = N_2 = 20000$  atoms,  $f_y = f_z = 150\text{ Hz}$ .

for  $f_x = 30\text{Hz}$ . Decreasing  $f_x$  to 6Hz increases the total number of domains from 7 to 17, whilst simultaneously reducing the peak density by a factor of  $\approx 2.5$ . The superfluid connection is monotonically increased such that below  $f_x \approx 17\text{Hz}$  the state can be considered in the SS-SS regime. The increasing number of domains can be explained simply by the BEC becoming longer, while the spin roton wavelength is roughly fixed by the confinement length in the direction of dipole polarization. This behavior starkly contrasts with that for droplet supersolids, which instead require a certain atom number for a given trap volume [23], and the supersolid regime is not possible if this criterion is not met [36–38]. For example, see the isolated droplets in Fig. 1(e), for which the atom number is insufficient for this trap to attain supersolidity.

*Conclusions.*— We predict a domain supersolid state in two-component dipolar condensates. This binary supersolid exists over a broad region of parameter space and, importantly, it is robust against the excitations caused by crossing the unmodulated BEC-to-domain supersolid phase transition. There is also a phase transition to an adjacent region where one of the components is supersolid but the other forms isolated domains. In contrast to single-component supersolids—which instead consist of relatively dense droplets—domain supersolids have similar peak densities as unmodulated BECs, and can pro-

duce numerous domains with relatively small atom numbers.

Our results are applicable to various dipole moment combinations, such as spin mixtures or binary gases comprised of two atomic species. Interestingly, we even find that a dipolar component can induce supersolidity within a non-dipolar component via their mutual interactions. Our work opens the door for future investigations into binary supersolid states and their excitations, as well as the exploration of novel 2D domain supersolids with exotic structures. Our results reveal a rich system that is within current experimental reach, and mark an important step towards long-lived bulk-supersolidity.

*Acknowledgements.*—We thank Danny Baillie and P. Blair Blakie for stimulating discussions. Part of the computational results presented here have been achieved using the HPC infrastructure LEO of the University of Innsbruck. T. B. acknowledges funding from FWF Grant No. I4426 RSF/Russia 2019. We acknowledge support of the Deutsche Forschungsgemeinschaft (DFG, German Research Foundation) under Germany’s Excellence Strategy – EXC-2123 QuantumFrontiers – 390837967, and FOR 2247.

- 
- [1] M. Boninsegni and N. V. Prokof’ev, Colloquium: Supersolids: What and where are they?, *Reviews of Modern Physics* **84**, 759 (2012).
- [2] J.-R. Li, J. Lee, W. Huang, S. Burchesky, B. Shteynas, F. Ç. Top, A. O. Jamison, and W. Ketterle, A stripe phase with supersolid properties in spin-orbit-coupled bose-einstein condensates, *Nature* **543**, 91 (2017).
- [3] T. M. Bersano, J. Hou, S. Mossman, V. Gokhroo, X.-W. Luo, K. Sun, C. Zhang, and P. Engels, Experimental realization of a long-lived striped bose-einstein condensate induced by momentum-space hopping, *Phys. Rev. A* **99**, 051602 (2019).
- [4] J. Léonard, A. Morales, P. Zupancic, T. Esslinger, and T. Donner, Supersolid formation in a quantum gas breaking a continuous translational symmetry, *Nature* **543**, 87 (2017).
- [5] L. Tanzi, E. Lucioni, F. Famà, J. Catani, A. Fioretti, C. Gabbanini, R. N. Bisset, L. Santos, and G. Modugno, Observation of a dipolar quantum gas with metastable supersolid properties, *Phys. Rev. Lett.* **122**, 130405 (2019).
- [6] F. Böttcher, J.-N. Schmidt, M. Wenzel, J. Hertkorn, M. Guo, T. Langen, and T. Pfau, Transient supersolid properties in an array of dipolar quantum droplets, *Phys. Rev. X* **9**, 011051 (2019).
- [7] L. Chomaz, D. Petter, P. Ilzhöfer, G. Natale, A. Trautmann, C. Politi, G. Durastante, R. M. W. van Bijnen, A. Patscheider, M. Sohmen, M. J. Mark, and F. Ferlaino, Long-lived and transient supersolid behaviors in dipolar quantum gases, *Phys. Rev. X* **9**, 021012 (2019).
- [8] G. Natale, R. van Bijnen, A. Patscheider, D. Petter, M. Mark, L. Chomaz, and F. Ferlaino, Excitation spectrum of a trapped dipolar supersolid and its experimental evidence, *Physical review letters* **123**, 050402 (2019).
- [9] L. Tanzi, S. Rocuzzo, E. Lucioni, F. Famà, A. Fioretti, C. Gabbanini, G. Modugno, A. Recati, and S. Stringari, Supersolid symmetry breaking from compressional oscillations in a dipolar quantum gas, *Nature* **574**, 382 (2019).
- [10] M. Guo, F. Böttcher, J. Hertkorn, J.-N. Schmidt, M. Wenzel, H. P. Büchler, T. Langen, and T. Pfau, The low-energy goldstone mode in a trapped dipolar supersolid, *Nature* **574**, 386 (2019).
- [11] L. Santos, G. Shlyapnikov, and M. Lewenstein, Roton-maxon spectrum and stability of trapped dipolar bose-einstein condensates, *Physical Review Letters* **90**, 250403 (2003).
- [12] Giovanazzi, S. and O’Dell, D. H.J., Instabilities and the roton spectrum of a quasi-1d bose-einstein condensed gas with dipole-dipole interactions, *Eur. Phys. J. D* **31**, 439 (2004).
- [13] L. Chomaz, R. M. W. van Bijnen, D. Petter, G. Faraoni, S. Baier, J. H. Becher, M. J. Mark, F. Wächtler, L. Santos, and F. Ferlaino, Observation of roton mode population in a dipolar quantum gas, *Nature Physics* **14**, 442 (2018).
- [14] J.-N. Schmidt, J. Hertkorn, M. Guo, F. Böttcher, M. Schmidt, K. S. Ng, S. D. Graham, T. Langen, M. Zwierlein, and T. Pfau, Roton excitations in an oblate dipolar quantum gas, *Physical Review Letters* **126**, 193002 (2021).
- [15] F. Böttcher, J.-N. Schmidt, J. Hertkorn, K. S. H. Ng, S. D. Graham, M. Guo, T. Langen, and T. Pfau, New states of matter with fine-tuned interactions: quantum droplets and dipolar supersolids, *Reports on Progress in Physics* **84**, 012403 (2020).
- [16] L. Chomaz, I. Ferrier-Barbut, F. Ferlaino, B. Laburthe-Tolra, B. L. Lev, and T. Pfau, Dipolar physics: A review of experiments with magnetic quantum gases, *arXiv preprint arXiv:2201.02672* (2022).
- [17] M. A. Norcia, C. Politi, L. Klaus, E. Poli, M. Sohmen, M. J. Mark, R. N. Bisset, L. Santos, and F. Ferlaino, Two-dimensional supersolidity in a dipolar quantum gas, *Nature* **596**, 357–361 (2021).
- [18] T. Bland, E. Poli, C. Politi, L. Klaus, M. A. Norcia, F. Ferlaino, L. Santos, and R. N. Bisset, Two-dimensional supersolidity in a circular trap, *arXiv preprint arXiv:2107.06680* (2021).
- [19] D. Baillie and P. B. Blakie, Droplet crystal ground states of a dipolar bose gas, *Phys. Rev. Lett.* **121**, 195301 (2018).
- [20] Y.-C. Zhang, F. Maucher, and T. Pohl, Supersolidity around a critical point in dipolar bose-einstein condensates, *Physical review letters* **123**, 015301 (2019).
- [21] Y.-C. Zhang, T. Pohl, and F. Maucher, Phases of supersolids in confined dipolar bose-einstein condensates, *Physical Review A* **104**, 013310 (2021).
- [22] J. Hertkorn, J.-N. Schmidt, M. Guo, F. Böttcher, K. S. H. Ng, S. D. Graham, P. Uerlings, T. Langen, M. Zwierlein, and T. Pfau, Pattern formation in quantum ferrofluids: From supersolids to superglasses, *Phys. Rev. Research* **3**, 033125 (2021).
- [23] E. Poli, T. Bland, C. Politi, L. Klaus, M. A. Norcia, F. Ferlaino, R. N. Bisset, and L. Santos, Maintaining supersolidity in one and two dimensions, *Phys. Rev. A* **104**, 063307 (2021).
- [24] A. Gallemí, S. Rocuzzo, S. Stringari, and A. Recati, Quantized vortices in dipolar supersolid bose-einstein-

- condensed gases, *Physical Review A* **102**, 023322 (2020).
- [25] S. Rocuzzo, A. Gallemí, A. Recati, and S. Stringari, Rotating a supersolid dipolar gas, *Physical review letters* **124**, 045702 (2020).
- [26] F. Ancilotto, M. Barranco, M. Pi, and L. Reatto, Vortex properties in the extended supersolid phase of dipolar bose-einstein condensates, *Physical Review A* **103**, 033314 (2021).
- [27] A. Trautmann, P. Ilzhöfer, G. Durastante, C. Politi, M. Sohmen, M. J. Mark, and F. Ferlaino, Dipolar quantum mixtures of erbium and dysprosium atoms, *Phys. Rev. Lett.* **121**, 213601 (2018).
- [28] G. Durastante, C. Politi, M. Sohmen, P. Ilzhöfer, M. J. Mark, M. A. Norcia, and F. Ferlaino, Feshbach resonances in an erbium-dysprosium dipolar mixture, *Phys. Rev. A* **102**, 033330 (2020).
- [29] C. Politi, A. Trautmann, P. Ilzhöfer, G. Durastante, M. Mark, M. Modugno, and F. Ferlaino, Interspecies interactions in an ultracold dipolar mixture, *Physical Review A* **105**, 023304 (2022).
- [30] H. Saito, Y. Kawaguchi, and M. Ueda, Ferrofluidity in a two-component dipolar bose-einstein condensate, *Phys. Rev. Lett.* **102**, 230403 (2009).
- [31] D. Scheiermann, L. A. Peña Ardila, T. Bland, R. N. Bisset, and L. Santos, Catalyzation of supersolidity in binary dipolar condensates, *arXiv preprint arXiv:2202.08259* (2022).
- [32] R. M. Wilson, C. Ticknor, J. L. Bohn, and E. Timmermans, Roton immiscibility in a two-component dipolar bose gas, *Phys. Rev. A* **86**, 033606 (2012).
- [33] A.-C. Lee, D. Baillie, P. Blakie, and R. Bisset, Miscibility and stability of dipolar bosonic mixtures, *Physical Review A* **103**, 063301 (2021).
- [34] R. N. Bisset, L. A. P. Ardila, and L. Santos, Quantum droplets of dipolar mixtures, *Phys. Rev. Lett.* **126**, 025301 (2021).
- [35] J. C. Smith, D. Baillie, and P. B. Blakie, Quantum droplet states of a binary magnetic gas, *Phys. Rev. Lett.* **126**, 025302 (2021).
- [36] H. Kadau, M. Schmitt, M. Wenzel, C. Wink, T. Maier, I. Ferrier-Barbut, and T. Pfau, Observing the rosenzweig instability of a quantum ferrofluid, *Nature* **530**, 194 (2016).
- [37] F. Wächtler and L. Santos, Quantum filaments in dipolar bose-einstein condensates, *Phys. Rev. A* **93**, 061603 (2016).
- [38] R. N. Bisset, R. M. Wilson, D. Baillie, and P. B. Blakie, Ground-state phase diagram of a dipolar condensate with quantum fluctuations, *Phys. Rev. A* **94**, 033619 (2016).
- [39] R. M. Wilson, C. Ticknor, J. L. Bohn, and E. Timmermans, Roton immiscibility in a two-component dipolar bose gas, *Physical Review A* **86**, 033606 (2012).
- [40] D. S. Petrov, Quantum mechanical stabilization of a collapsing bose-bose mixture, *Phys. Rev. Lett.* **115**, 155302 (2015).
- [41] Contrast  $C_\sigma$  is calculated by considering a line of maximum density in the  $z = 0$  plane, defined by the maximum density along  $y$  for each value of  $x$ . The contrast is then taken to be the largest value of neighboring density max/min pairs along this line, as demonstrated graphically in the Supplemental Material [42].
- [42] Supplemental Materials, doi to be added.
- [43] <https://youtu.be/jUxQCBEZiZM>.
- [44] P. Ilzhöfer, M. Sohmen, G. Durastante, C. Politi,
- A. Trautmann, G. Natale, G. Morpurgo, T. Giamarchi, L. Chomaz, M. Mark, *et al.*, Phase coherence in out-of-equilibrium supersolid states of ultracold dipolar atoms, *Nature Physics* **17**, 356 (2021).

## Supplemental materials: Domain supersolids in binary dipolar condensates

T. Bland, E. Poli, L. A. Peña Ardila, L. Santos, F. Ferlaino, and R. N. Bisset

### Density contrast

The supersolid quality is measured through the density contrast, akin to interferometric visibility, defined as

$$\mathcal{C}_\sigma = \frac{n_\sigma^{\max} - n_\sigma^{\min}}{n_\sigma^{\max} + n_\sigma^{\min}} \quad (\text{S1})$$

for each bosonic component  $\sigma = \{1, 2\}$  and where  $n_\sigma^{\max}$  and  $n_\sigma^{\min}$  are neighboring maxima and minima in the 3D density as one moves along the long direction of the trap. In Fig. S1 we graphically depict the line of maximum 3D density in the  $z = 0$  plane, showing the maxima (red circles) and minima (green crosses) in the density along this curve. Typically, for the component with a larger dipole moment this curve lies along  $y = 0$ , just as it does for droplet supersolids [5–7]. However, the nondipolar component has a greater superfluid connection along the rails, a feature which is captured by our generalization of Eq. (S1). This connection can still be lost however, through tightening  $f_y$ , for example.

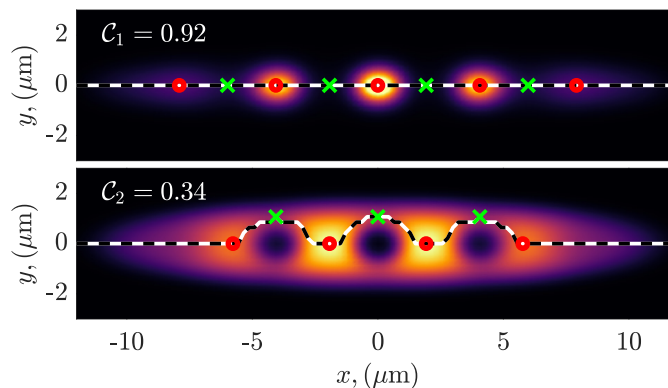


FIG. S1. Contrast  $\mathcal{C}_\sigma$  of a dipolar-nondipolar mixture of  $^{164}\text{Dy}$  atoms. Dashed line indicates the  $y$  position of the maximum density along  $x$ . Red circles are the peaks ( $n_\sigma^{\max}$ ) and green crosses the troughs ( $n_\sigma^{\min}$ ) of density along the dashed line. Other parameters:  $(\mu_1, \mu_2) = (-10, 0)\mu_B$ ,  $N_1 = N_2 = N/2 = 7000$ ,  $a_{12} = 70a_0$ ,  $a_{11} = a_{22} = 100a_0$ ,  $(f_x, f_y, f_z) = (21, 150, 150)\text{Hz}$ .

### Dynamic preparation

The preparation of a droplet supersolid has been achieved through either taking an unmodulated BEC and quenching the scattering length across the unmodulated BEC-to-supersolid transition [5–7], or by direct evaporative cooling into the droplet supersolid state [7, 17, 18]. The two-component case affords a wide range of possibilities for domain supersolid preparation, due to the large number of tunable interaction parameters in the system. Here, we investigate one possibility through tuning the intercomponent scattering length  $a_{12}$ . Taking an initially unmodulated miscible dipolar-nondipolar mixture with the parameters from Fig. S1 and  $a_{12} = 65a_0$  we simulate an instantaneous quench to  $a_{12} = 70a_0$ . The consequent dynamics are shown in Fig. S2. Despite the violent nature of the instantaneous quench, the system maintains phase coherence throughout the lifetime of the simulation, as indicated by the blue (red) isosurface for component 1 (2), and the solution resembles the target stationary solution [Fig. S1]. We also include a Supplementary Video of the dynamics [43].

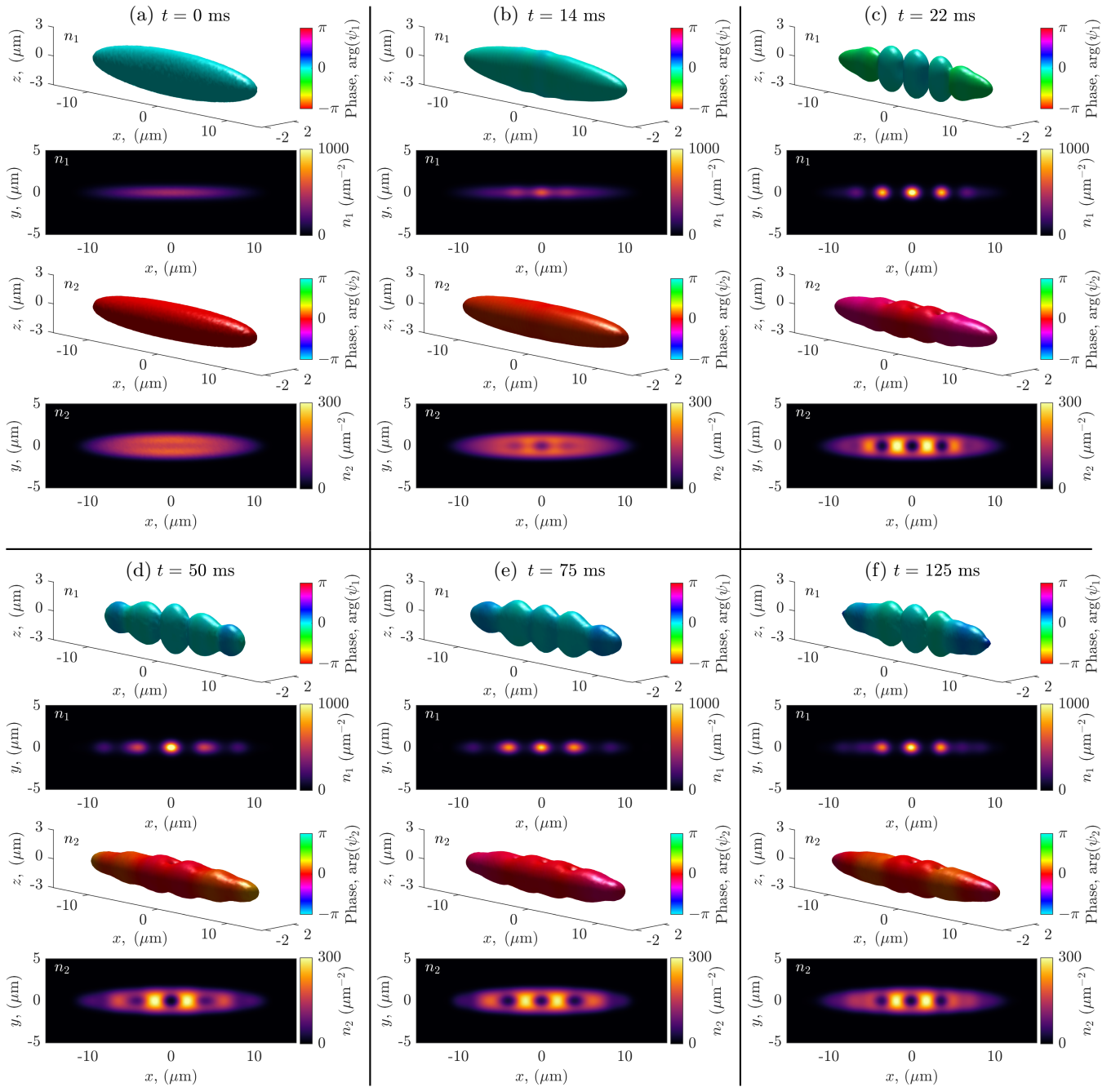


FIG. S2. Preparation of a domain supersolid through an interaction quench. Simulation of an instantaneous quench from  $a_{12} = 65a_0$  to  $a_{12} = 70a_0$  at  $t = 0$ , with other parameters from Fig. S1. Each labeled frame corresponds to a time during the consequent dynamics, and within each frame the data can be understood row-by-row. Row 1: 5% density isosurface for component 1 colored to the phase, and centered such that the phase at the origin is 0, perfect coherence for component 1 would be light blue. Row 2: Column density for component 1 normalized to peak value over the whole simulation. Row 3: same as Row 1 but for the second component, but perfect coherence in component 2 would be red. Row 4: same as Row 2 but for the second component, with a smaller peak density. Note that the stationary solution for the final parameters is the state presented in Fig. S1. A Supplementary Video of this simulation is also included [43].

We can dynamically measure the supersolid quality by plotting the time dependent phase coherence over time. Following Ref. [5] (see also Refs. [18, 44]) we define the phase coherence as

$$\alpha_\sigma = 1 - \frac{2 \int_{\mathcal{R}} dx dy |\psi_\sigma(x, y)|^2 |\theta_\sigma(x, y) - \beta|}{\int_{\mathcal{R}} dx dy |\psi_\sigma(x, y)|^2}, \quad (\text{S2})$$

where  $\theta_\sigma(x, y)$  is the phase of  $\psi_\sigma(x, y)$  in the  $z = 0$  plane, and  $\beta$  is a fitting parameter to maximize  $\alpha_\sigma$  at each time. The integration region  $\mathcal{R}$  encompasses the cloud. From this definition  $\alpha_\sigma = 1$  corresponds to perfect phase coherence across the BEC. In Fig. S3 we present the dynamical evolution of the phase coherence after the instantaneous quench presented in Fig. S2. Throughout the total time evolution,  $\alpha_\sigma$  does not go below 0.85 for either component, suggesting excellently maintained phase coherence.

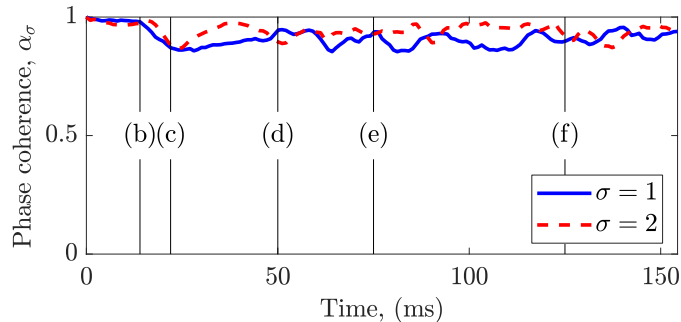


FIG. S3. Phase coherence  $\alpha_\sigma$  for each component  $\sigma = \{1, 2\}$  following an instantaneous quench from an unmodulated miscible BEC to a domain supersolid state. Labels in the plot coincide with the frames shown in Fig. S2.